

GEOMETRIC CAMERA CALIBRATION OF THE BiLSAT SMALL SATELLITE: PRELIMINARY RESULTS

J. Friedrich *, U. M. Leloğlu, E. Tunali

TÜBİTAK BİLTEN, ODTU Campus, 06531 Ankara, Turkey - (jurgen.friedrich, leloglu, tunali)@bilten.metu.edu.tr

Commission I, WG 6

KEY WORDS: Geometric, Camera, Calibration, Target point, Aerial photo, Topographic map, UTM coordinate, SRTM heights

ABSTRACT:

The interior geometric calibration of the multi-spectral camera of BiLSAT satellite is aimed using three sets of images from Ankara. Each set contains four different images for channels Red, Green, Blue (RGB), and Near Infra Red (NIR) in which well-defined target points were identified and their image coordinates measured. The target points' UTM coordinates were extracted from aerial photos or topographic maps and collected from field using hand-held GPS receiver. A least square parameter estimation was then applied to fit the image coordinates to the UTM coordinates and heights from the SRTM 90 m elevation model, thereby computing best estimates for the camera position and orientation as well as all the required geometric camera calibration parameters. These parameters were then analyzed and compared to each other. The obtained results show that the focal length f has a value of about $f=179$ mm. Further, the principal point coordinates and radial lens distortions have a maximum of about ten pixels.

1. INTRODUCTION

BiLSAT earth observing satellite has been built in the framework of a technology transfer program between SSTL, Guildford, UK and TÜBİTAK-BİLTEN, Ankara, Turkey. Since its launch on Sept. 27, 2003 to its sun-synchronous orbit at 686 km, it is being operated from the ground station in Ankara. BiLSAT has a panchromatic camera with a 12.7 m ground sampling distance (GSD), and four separate cameras sensitive to red, green, blue and NIR bands, together forming a multi-spectral camera with a 27.6 m GSD. The geometric calibration of the cameras was not performed on the ground, so the parameters need to be estimated in-orbit. In this work, a study to determine interior camera parameters of BILSAT multi-spectral camera and the first results from the study are presented.

BiLSAT carries three imagers on board. The imager named ÇOBAN is out of the scope of this study, so it will not be discussed. The other two imagers are multi-spectral imager and panchromatic imager. The radiometric calibration study has only been made for multi-spectral camera, so only this imager will be discussed.

BiLSAT imagers are based on "Modular Camera" approach. The Modular Camera forms the basis of the area array camera of BiLSAT imagers. The Modular camera is a single channel unit, and is used in single configuration for a panchromatic camera, and as multiple units for a Multi-spectral imager. Multi-spectral camera is made of four physically different cameras. Multi-spectral imager was constructed by using four modular cameras with appropriate lenses and filters. In the modular camera, KAI 4000M CCDs were used. The specifications of the CCD are given in Table 1.

Table 1: KODAK KAI 4000M CCD specifications

Number of pixels	4.2 million pixels, 2048 (H) by 2048 (V)
Pixel size	7.4 mm square pixels
Scanning	Progressive scan (non-interlaced)
Outputs	Four video outputs, one at each corner of the sensor
Imaging area	15.2 mm x 15.2 mm imaging area
Shutter	Electronic shutter
Dark Current	0.5 10 ⁻⁵ A/m ² at 40° C
Anti-blooming protection	Exists

Interior camera parameters specify geometric camera properties, such as (Mikhail et al. 2001)

- The principal distance f , the distance between the camera's focal point and the image plane, with its x, y components f_x and f_y ,
- The coordinates of the principal point Δx and Δy in pixels,
- Effective pixel size c , and

* Corresponding author.

- Radial lens distortion given by k_1 and k_2 .

Using these interior parameters, the corrected coordinates x' and y' of an image point in a metric system are given by

$$\begin{aligned}\bar{x} &= c(x - \Delta x), \quad \bar{y} = c(y - \Delta y), \\ x' &= \bar{x} \left(1 + k_1 r^2 + k_2 r^4 \right), \\ y' &= \bar{y} \left(1 + k_1 r^2 + k_2 r^4 \right), \\ r &= c \sqrt{(x - \Delta x)^2 + (y - \Delta y)^2},\end{aligned}\tag{1}$$

where x and y are the measured image coordinates in pixels, and c is the effective pixel size, which is the size factor of a pixel to the chosen metric system.

Exterior camera parameters describe the spatial relation between the camera and the world coordinate systems. Exterior parameters are

- A rotation matrix R with 3 sequential rotations angles ω , φ , κ (roll, pitch, and yaw) about the x , y , and z -axis, describing the camera orientation in the world coordinate system, and
- A translation vector t_0 with 3 Cartesian coordinates X_0 , Y_0 , Z_0 describing the camera position, which is the camera's principal point, in the world coordinate system.

Applying the usual pinhole camera model and the equation for the undistorted central projection, the relation between an image point with corrected coordinates x' , y' and its corresponding 3D world point with Cartesian coordinates X , Y , Z are given by

$$\begin{aligned}x' &= -f_x \frac{R_{11}(X - X_0) + R_{21}(Y - Y_0) + R_{31}(Z - Z_0)}{R_{13}(X - X_0) + R_{23}(Y - Y_0) + R_{33}(Z - Z_0)}, \\ y' &= -f_y \frac{R_{12}(X - X_0) + R_{22}(Y - Y_0) + R_{32}(Z - Z_0)}{R_{13}(X - X_0) + R_{23}(Y - Y_0) + R_{33}(Z - Z_0)},\end{aligned}\tag{2}$$

where the rotation matrix has the following components using $R = R_x(\omega) R_y(\varphi) R_z(\kappa)$

$$R = \begin{bmatrix} \cos \varphi \cos \kappa & -\cos \varphi \sin \kappa & \sin \varphi \\ \sin \omega \sin \varphi \cos \kappa + \cos \omega \sin \kappa & -\sin \omega \sin \varphi \sin \kappa + \cos \omega \cos \kappa & -\sin \omega \cos \varphi \\ -\cos \omega \sin \varphi \cos \kappa + \sin \omega \sin \kappa & \cos \omega \sin \varphi \sin \kappa + \sin \omega \cos \kappa & \cos \omega \cos \varphi \end{bmatrix}.\tag{3}$$

Inserting Eqs.(1) into (2) results in the general observation equations of the geometric camera calibration

$$\begin{aligned}x &= \frac{1}{1 + k_1 r^2 + k_2 r^4} \left[\Delta x - \frac{f_x}{c} \frac{R_{11}(X - X_0) + R_{21}(Y - Y_0) + R_{31}(Z - Z_0)}{R_{13}(X - X_0) + R_{23}(Y - Y_0) + R_{33}(Z - Z_0)} \right], \\ y &= \frac{1}{1 + k_1 r^2 + k_2 r^4} \left[\Delta y - \frac{f_y}{c} \frac{R_{12}(X - X_0) + R_{22}(Y - Y_0) + R_{32}(Z - Z_0)}{R_{13}(X - X_0) + R_{23}(Y - Y_0) + R_{33}(Z - Z_0)} \right].\end{aligned}\tag{4a}$$

or shorter

$$x = \frac{1}{e_1} \left[\Delta x - \frac{f_x}{c} \frac{R_1^T t_0}{R_3^T t_0} \right], \quad y = \frac{1}{e_2} \left[\Delta y - \frac{f_y}{c} \frac{R_2^T t_0}{R_3^T t_0} \right].\tag{4b}$$

For a least square estimation (LSE) of the intrinsic and extrinsic camera parameters, the partial derivatives of Eq.(4) are needed and given by (only non-zero derivatives are listed below)

$$\frac{\partial x}{\partial \Delta x} = \frac{1}{e_1}, \quad \frac{\partial y}{\partial \Delta y} = \frac{1}{e_2},\tag{5}$$

$$\frac{\partial x}{\partial f} = \frac{-1}{c e_1} \frac{R_1^T t_0}{R_3^T t_0}, \quad \frac{\partial y}{\partial f} = \frac{-1}{c e_2} \frac{R_2^T t_0}{R_3^T t_0},$$

$$\frac{\partial x}{\partial k_1} = \frac{r^2}{e_1^2} \frac{f_x}{c} \frac{R_1^T t_0}{R_3^T t_0}, \quad \frac{\partial y}{\partial k_1} = \frac{r^2}{e_2^2} \frac{f_y}{c} \frac{R_2^T t_0}{R_3^T t_0},$$

$$\frac{\partial x}{\partial k_2} = \frac{r^4}{e_1^2} \frac{f_x}{c} \frac{R_1^T t_0}{R_3^T t_0}, \quad \frac{\partial y}{\partial k_2} = \frac{r^4}{e_2^2} \frac{f_y}{c} \frac{R_2^T t_0}{R_3^T t_0},$$

$$\frac{\partial x}{\partial X_0} = \frac{f_x}{c e_1} \frac{R_{11} R_3^T t_0 - R_{13} R_1^T t_0}{(R_3^T t_0)^2}, \quad \frac{\partial y}{\partial X_0} = \frac{f_y}{c e_2} \frac{R_{12} R_3^T t_0 - R_{13} R_2^T t_0}{(R_3^T t_0)^2},$$

$$\frac{\partial x}{\partial Y_0} = \frac{f_x}{c e_1} \frac{R_{21} R_3^T t_0 - R_{23} R_1^T t_0}{(R_3^T t_0)^2}, \quad \frac{\partial y}{\partial Y_0} = \frac{f_y}{c e_2} \frac{R_{22} R_3^T t_0 - R_{23} R_2^T t_0}{(R_3^T t_0)^2},$$

$$\frac{\partial x}{\partial Z_0} = \frac{f_x}{c e_1} \frac{R_{31} R_3^T t_0 - R_{33} R_1^T t_0}{(R_3^T t_0)^2}, \quad \frac{\partial y}{\partial Z_0} = \frac{f_y}{c e_2} \frac{R_{32} R_3^T t_0 - R_{33} R_2^T t_0}{(R_3^T t_0)^2},$$

$$\begin{aligned} \frac{\partial x}{\partial \omega} &= \frac{-f_x}{c e_1} \frac{(\cos \omega \sin \varphi \cos \kappa - \sin \omega \sin \kappa)(Y - Y_0) + (\sin \omega \sin \varphi \cos \kappa - \cos \omega \sin \kappa)(Z - Z_0)}{(R_3^T t_0)} \\ &\quad - \frac{f_x}{c e_1} \frac{\cos \varphi [\cos \omega (Y - Y_0) + \sin \omega (Z - Z_0)] R_1^T t_0}{(R_3^T t_0)^2}, \end{aligned}$$

$$\begin{aligned} \frac{\partial y}{\partial \omega} &= \frac{f_y}{c e_2} \frac{(\cos \omega \sin \varphi \sin \kappa - \sin \omega \cos \kappa)(Y - Y_0) + (\sin \omega \sin \varphi \sin \kappa - \cos \omega \cos \kappa)(Z - Z_0)}{(R_3^T t_0)} \\ &\quad - \frac{f_y}{c e_2} \frac{\cos \varphi [\cos \omega (Y - Y_0) + \sin \omega (Z - Z_0)] R_2^T t_0}{(R_3^T t_0)^2}, \end{aligned}$$

$$\begin{aligned} \frac{\partial x}{\partial \varphi} &= \frac{f_x}{c e_1} \frac{\cos \kappa [\sin \varphi (X - X_0) - \sin \omega \cos \varphi (Y - Y_0) + \cos \omega \cos \varphi (Z - Z_0)]}{(R_3^T t_0)} \\ &\quad + \frac{f_x}{c e_1} \frac{[\cos \varphi (X - X_0) + \sin \omega \sin \varphi (Y - Y_0) - \cos \omega \sin \varphi (Z - Z_0)] R_1^T t_0}{(R_3^T t_0)^2}, \end{aligned}$$

$$\begin{aligned} \frac{\partial y}{\partial \varphi} &= \frac{-f_y}{c e_2} \frac{\sin \kappa [\sin \varphi (X - X_0) - \sin \omega \cos \varphi (Y - Y_0) + \cos \omega \cos \varphi (Z - Z_0)]}{(R_3^T t_0)} \\ &\quad + \frac{f_y}{c e_2} \frac{[\cos \varphi (X - X_0) + \sin \omega \sin \varphi (Y - Y_0) - \cos \omega \sin \varphi (Z - Z_0)] R_2^T t_0}{(R_3^T t_0)^2}, \end{aligned}$$

$$\frac{\partial x}{\partial \kappa} = \frac{f_x}{c e_1 R_3^T t_0} \left[\begin{array}{l} \cos \varphi \sin \kappa (X - X_0) + (\sin \omega \sin \varphi \sin \kappa - \cos \omega \cos \kappa)(Y - Y_0) \\ - (\cos \omega \sin \varphi \sin \kappa + \sin \omega \cos \kappa)(Z - Z_0) \end{array} \right],$$

$$\frac{\partial y}{\partial \kappa} = \frac{f_y}{c e_2 R_3^T t_0} \left[\begin{array}{l} \cos \varphi \cos \kappa (X - X_0) + (\sin \omega \sin \varphi \cos \kappa + \cos \omega \sin \kappa)(Y - Y_0) \\ - (\cos \omega \sin \varphi \cos \kappa - \sin \omega \sin \kappa)(Z - Z_0) \end{array} \right].$$

2. PARAMETER ESTIMATION

Parameters are computed by a least square estimation (LSE). The LSE minimizes the sum of the squared residuals e_k multiplied by the weight W_k of an observation (Koch 1999),

$$\sum_{k=1}^n e_k W_k e_k = \min, \quad (6)$$

where n is the total number of observations. This principle leads to an iterative scheme to estimate parameters β_{i+1} where u is the total number of parameters given by

$$\begin{aligned} \beta_{i+1} &= \beta_i + \Delta \beta_i = \beta_i + (X^T W X)^{-1} X^T W y_j, \\ y_j &= y_j^{\text{Obs}} - y_j^0, \end{aligned} \quad (7)$$

where X is a $(n \times u)$ matrix of partial derivatives $(\partial y_j / \partial \beta_i)_0$ according to Eq.(5), and y_j the differences between the observed and computed image coordinates obtained through Eq.(4) in combination with the approximate parameters β_i . In this application, all observations have the same weight $W_k = 1$, and the iteration in Eq.(7) was stopped when all residuals e_k became smaller than a given limit, here 0.2 pixel or about 5 m. This limit was generally reached after 2 iterations. Since the orbital height of the satellite is already available, this information is also used as a constraint in the optimization procedure.

3. DATA ACQUISITION

From all available Ankara images the one with the best quality was selected in the beginning to estimate geometric calibration parameters in order to obtain the highest possible accuracy. This was the green channel image of Ankara on February 1st, 2004. In doing this, it's also assumed that the images of other channels have similar (but different) geometric calibration parameters.

After identifying good visible target points and measuring their coordinates in the image mostly located close to highways and larger roads in Ankara, a serious problem was encountered with the topographic maps because the available ones are sometimes older than 20 years, not up-to-date and therefore not very suitable for the purpose of this work. A much better alternative was found in an adequate set of geo-referenced aerial photos of Ankara with sub-meter precision. In these photos, the target points' UTM coordinates were extracted and their heights computed with the SRTM 90 m elevation model, and then transferred to the WGS-84 system, thus providing the Cartesian X, Y, Z coordinates in Eq.(2). In addition, GPS measurements were taken at other target points to collect further data. Since the error of GPS measurements are at the level of a fraction of the GSD, they are directly used.

Since the release of the Shuttle Radar Topography Mission (SRTM) global elevation data in 2003 (<http://edftp.cr.usgs.gov/pub/data/srtm/>), continuous height data was available at least for America and Eurasia as of 2003. The absolute accuracy of SRTM heights at low vegetation areas is better than the SRTM mission specifications of 16 m (Sun et al. 2003).

Nevertheless, it was thought to be a good check and control of the acquired data and the estimation procedure to use also a less quality input data set obtained from topographic maps. Therefore, two sets of data were compiled as:

- 1) "utm24.txt" with 24 target points based on topographic maps, and
- 2) "utm38.txt" with 38 target points based on aerial photos and GPS measurements.

The location of the 38 target points is shown in Figure 1.

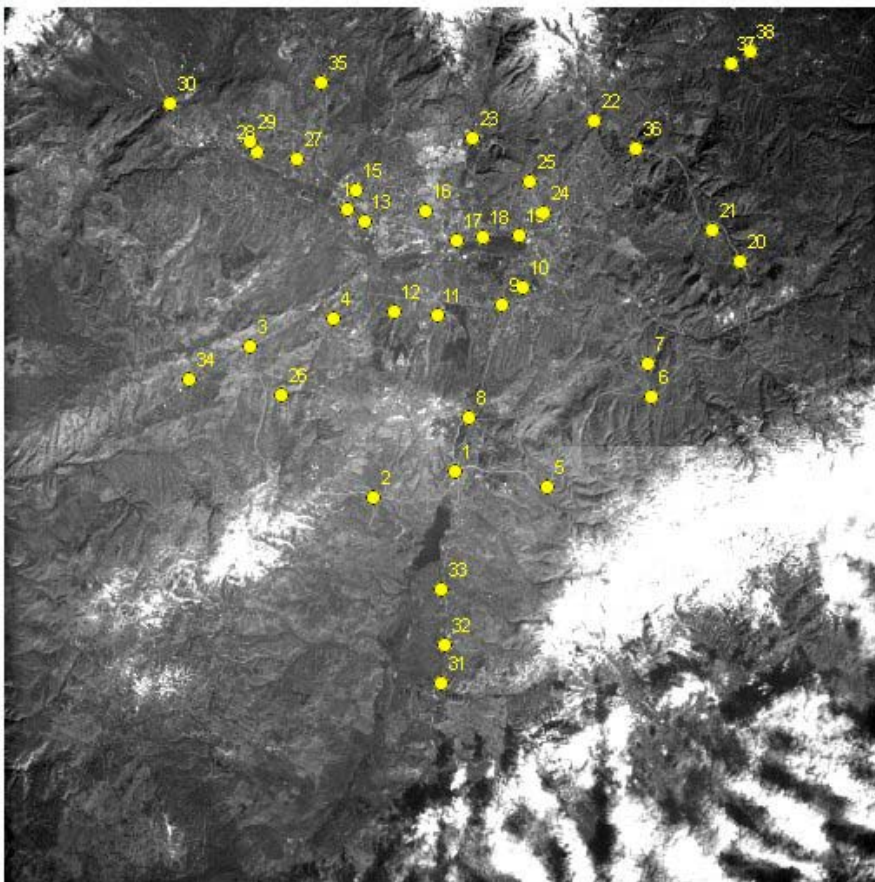


Figure 1: Target points in the green channel image of Ankara February 1st, 2004

4. RESULTS OF PARAMETER ESTIMATION

The estimation results for both data sets after 2 iterations are given in Tables 2 and 3.

Table 2: LSE results for the “utm24.txt” data set

Position	ECEF coordinates	D-params	+/-Std.Dev.	[All m]
X0	4575564.383	284.071	0.659	
Y0	2963858.634	982.370	0.451	
Z0	4531353.696	976.172	0.678	
Lat, Lon, Height				
	32.93347	39.90257	686462.221	[deg, deg, m]
Orientation				
Angles in ECEF system	D-params	+/-Std.Dev.	[All deg]	
Omega	-32.954493	-0.000356	0.000001	
Phi	40.209733	0.000000	0.000000	
Kappa	127.118701	0.000002	0.000012	
Position				
Inner Camera Params	D-params	+/-Std.Dev.	[m, pix, pix, 2x no dim.]	
f	0.1790	0.00000	0.00000	
dx	-0.12900	-0.00170	0.00020	
dy	0.09130	-0.00110	0.00030	
k1	-0.08310	-0.10430	0.00960	
k2	-0.07020	-0.12950	0.01630	

Table 3: LSE results for the “utm38.txt” data set

Position	ECEF coordinates	D-params	+/-Std.Dev.	[All m]
X0	4566818.048	4.483	0.043	
Y0	2906651.754	-33.472	0.024	
Z0	4532525.442	20.786	0.044	
Lat, Lon, Height				
	32.47561	40.10931	686051.883	[deg, deg, m]
Orientation				
Angles in ECEF system	D-params	+/-Std.Dev.	[All deg]	
Omega	-32.860784	0.033459	0.000024	
Phi	40.152602	-0.000072	0.000021	
Kappa	127.098838	-0.001125	0.000365	
Position				
Inner Camera Params	D-params	+/-Std.Dev.	[m, pix, pix, 2x no dim.]	
f	0.1788	0.0000	0.0000	
dx	11.7464	-0.0586	0.0077	
dy	-8.4191	0.1591	0.0094	
k1	-0.0512	0.3178	0.0470	
k2	1.1417	1.1921	0.0400	

The column “D-params” shows the differences $\Delta\beta_i$ in the last iteration of Eq.(7).

5. DISCUSSION OF RESULTS

All results were obtained by separate parameter estimations in three steps one after the other using identical data in the following sequence:

- 1) Position parameters of camera (X_0, Y_0, Z_0),
- 2) Orientation parameters of camera (ω, φ, κ), and
- 3) Inner camera parameters (focal length f , principal point coordinates $\Delta x, \Delta y$, and lens distortion parameters k_1, k_2).

As can be seen in Table 2 and 3, the results in both tables are similar. In both, the focal length f has a value of about $f = 179$ mm. Further, the principal point coordinates and radial lens distortions have a maximum of about ten. The qualities of both data sets are more or less the same when comparing the results in Table 2 and 3.

Other tests with the same data sets have also shown that the applied estimation procedure is very sensitive to the camera position. Besides the refraction had only a very small impact on the results, mainly because the used image is taken in a close-to-nadir direction. But, this also caused some problems in the calibration process due to small variation in depth. For that reason, in future, more oblique images will be obtained and the study will be repeated. Besides, the GCPs are concentrated in the centre of the image and this reduces the accuracy of the results. Hence, more GCPs will be collected especially at the corners of the images.

REFERENCES

- Am. Soc. of Photogrammetry (1996) Manual of Photogrammetry, 4th ed., 1056 p.
Koch, K-R. (1999) Parameter Estimation and Hypothesis Testing in Linear Models. Springer Verlag, 378 p.
Mikhail, E.M., McGlone, C., Bethel, J.S. (2001) Introduction to Modern Photogrammetry, John Wiley & Sons, New York, 496 p.
Sun, G., Ranson, K.J., Kharuk, V.I. and K. Kovacs. Validation of surface height from shuttle radar topography mission using shuttle laser altimeter. Remote Sensing of Environment Vol.88, 2003, pp.401-411.